Published in IET Microwaves, Antennas & Propagation
Received on 9th May 2014
Revised on 24th August 2014
Accepted on 14th September 2014
doi: 10.1049/iet-map.2014.0308

ISSN 1751-8725

Beamforming properties and design of the phased arrays in terms of irregular subarrays

Zi-Yuan Xiong, Zhen-Hai Xu, Shun-Ping Xiao

State Key Laboratory of Complex Electromagnetic Environment Effects on Electronics and Information System, National University of Defense Technology, Changsha 410073, People's Republic of China
E-mail: ziyuanxiong@gmail.com

Abstract: Large phased arrays are often organised by subarrays given the current state of technology. The irregular subarray architecture, which can effectively mitigate the quantisation lobes, has received a renewed interest in recent years. Recent researches present some innovative particular irregular subarrays to provide practical means to eliminate the quantisation lobes using several (even only one) kinds of subarray. However, there is no single, neat theory of the irregularly partitioned array antennas in the literature. This study presents some derivations of the beamforming properties for arrays with arbitrary subarray partition to fill this gap. Derivations have led us to introduce a novel approach to assess the radiation properties which is useful for the systematic design of phased arrays. Numerical experiments are carried out to validate the authors' derivations. Additionally, an elaborate example illustrates a design discipline for a limited-field-of-view array with polyomino-shaped subarrays.

1 Introduction

Large phased array antennas are very expensive to build given the current state of technology [1–3]. In practice, elements of array antennas are usually partitioned to form several subarrays. Such technology reduces the number of controls, which is a very effective way to reduce the complexity of the architecture, the costs, as well as the occupied physical space (e.g. on aircraft, satellite etc.) [4–7].

Although using subarrays is an effective way to achieve a tradeoff between performance and cost, it is complicated to optimise the subarray configuration. Besides, a smart partitioning of a very large planar array into a number of separately fed subarrays offers many interesting design possibilities in antenna synthesis problems [8–11]. A general conclusion is that the regularly partitioning always brings huge grating lobes (for both narrow-band and wide-band arrays) which deteriorate the sidelobe level of the scanning or simultaneous beams [6, 12, 13]. Various subarray techniques have been developed to reduce these lobes, such as irregular or aperiodic subarray partitioning, interlaced and overlapped subarrays. The aperture of overlapped subarray is relatively large (the completed overlapped subarray can even employ the whole aperture of antenna [14]). Thus the better subarray pattern, such as the 'flat-topped pattern', can be approximately obtained [15, 16]. The rationale of interlaced or overlapped subarrays have been understood for years and already demonstrated in practice [17]. Recently, the mathematics theory of the design of overlapped subarray is presented in [18] in a signal-processing viewpoint. However, the interlaced or overlapped subarrays are relatively difficult and costly to build [6, 17, 19]. The irregular-shaped subarray partitioning is relatively easily realised and has been studied for many years [1, 20, 21]. The primary principle of the irregular subarray is that the irregular shapes can break the periodicity of the phase-centre locations. Considering the modularisation is a popular property in design and manufacture, especially for the large arrays, several subarray architectures have been proposed, such as the aperiodic array antenna using diamond tile-shaped subarrays [22], Penrose tile-shaped subarrays [8, 23, 24], pinwheel tile-shaped subarrays [23, 25] and so on. Note that using these subarrays always requires the aperiodic arrangement of array elements. In fact, for the regularly arranging elements (i.e. elements are arranged at the lattice), one can also design the particular subarrays which are convenient for the module production. The relevant research was first described by Mailloux [19, 26], who had introduced the polyomino structure to design subarrays. In [7], this paper has been developed for arbitrary lattice structure and the polyhex-shaped subarrays have been used. Using the polyomino or polyhex-shaped subarrays, one can 'exactly fill' or 'tile' the array plane (i.e. without any overlaps and holes). The irregularity, involved the exactly filling process, makes the array migrating the quantisation lobes. A solver of the exactly filling partition is developed based on the exact cover theory in [7]. It has been recognised that the exactly filling partition is one of the nondeterministic polynomial time (NP)-complete problems [7], which means that it is impossible to find the solution by hand for a large array. There could be astronomical number of partitioning strategies. Thus, it is necessary to use a convenient performance evaluating method for the beamforming to design the irregular subarray partition. However, the analysis and systematic design of phased arrays with irregular subarrays are absent

from the publications, even though for the linear arrays [27]. Using the data-compression techniques to assess the sidelobe level is an interesting and good try [28]. This paper focuses on the design of subarray partition. Analysis of the beamforming properties of the subarrayed antennas, especially the irregular-shaped subarray partitioning, is developed.

The outline of this paper is as follows. In Section 2, typical applications of the beamforming technique at subarray level are given. Then the generic mathematics formulation for beamforming is established and the optimal phase control method is deduced. Examples are represented to demonstrate the predominance of the phase control method. In Section 3, a novel approach to assess the beamforming properties based on the established beamforming model is presented. Two typical requirements for the beam scanning – a minimum gain requirement and a sidelobe level requirement – are analysed. A selected set of numerical results to illustrate the limited-field-of-view (LFOV) technology and validate the analyses are also given in this section. In Section 4, an elaborate design instance of subarray configuration is demonstrated. Finally, some conclusions and perspectives are given in Section 5.

2 Beamforming technology for subarrayed antennas

2.1 Background

The ability of rapid and flexible beam scanning is the primary advantage of the array antennas. Such ability is widely required and used in these applications: LFOV (or limited scanned arrays), wide-band and wide-angle scanning (WBWS) arrays and multiple simultaneous beam (MSB) beamforming etc.

LFOV beamforming technology has been employed in lots of real systems, such as the aerodrome radar stations for air traffic control and instrumental landing of aeroplanes [16]; automotive radars designed for preventing collisions [29]; shipboard fire-control radars; systems of satellite communications, in particular, for synchronous satellites, the earth subtends a conical angle of 8.7° half angle [16, 30]. Other satellite systems sometimes scan a high-directivity beam over even smaller angles to do detailed mapping [30]. Besides, fast electrical scanning in a narrow sector can also be combined with wide-angle mechanical rotation of the whole array.

The radar and communications applications brought in requirements for wide-band performance [14, 31]. An effective approach to fulfill the wide-band scanning is using the subarrays with phase shifters at the element level and the time delays at each subarray input.

Visually, typical subarray structures for beamforming are shown in Fig. 1. In Fig. 1*a*, there is only a single phase shifter per subarray, which is the scheme of LFOV described in [12, 14]. Fig. 1*b* shows the WBWS technique realised by subarrayed antennas. The phase shifters arranged at the element level are used to steer the main beam at the centre frequency, whereas the time delays added at subarray level are used to generate correct time delay for all frequencies at the main beam direction. Fig. 1*c* gives a more flexible subarray configuration with digital beam forming networks at subarray level. The networks can also introduce time delay or phase shift. Additionally, MSBs are typically formed by digitally combining the subarrays to form beams in the required directions within the region of interest [32].

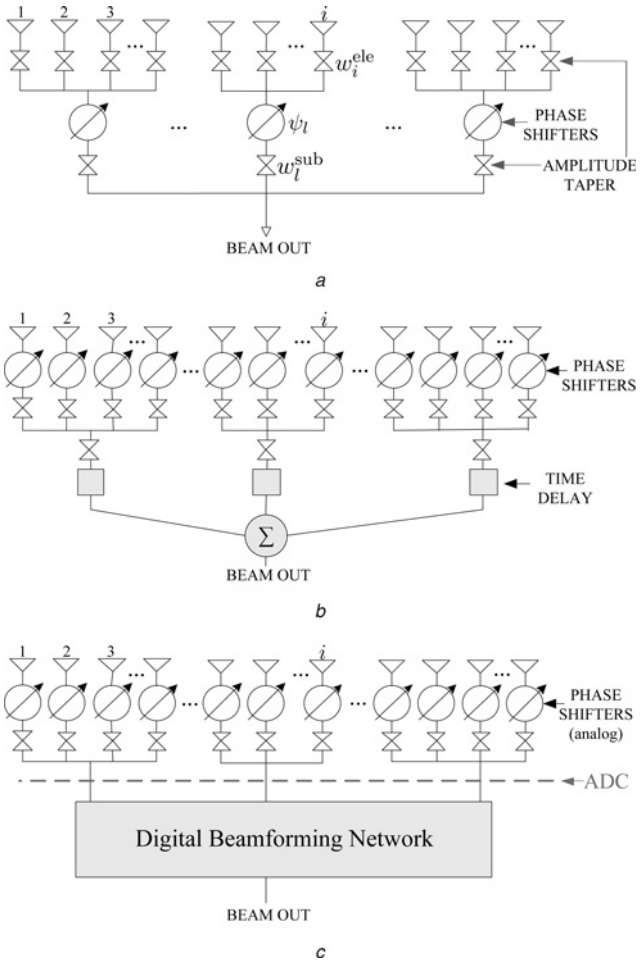

Fig. 1 *Subarray configuration of the beamforming techniques of*
a LFOV
b WBWS
c MSBs

It has been recognised that the LFOV and WBWS applications for subarray technology exhibit similar behaviour and suffer the same deficiencies [30]. In fact, the above-mentioned applications (LFOV, WBWS and MSB) place similar requirements on subarray technology and array architecture. The following analyses are applicable to these beamforming techniques.

2.2 Mathematical formulation

For mathematical convenience, the electromagnetic component at the ith element with location $\boldsymbol{r}_i$ for an incident wave can be expressed as $\boldsymbol{E}\,e^{j(2\pi ft+\boldsymbol{k}^T\boldsymbol{r}_i)}$, where $\boldsymbol{E}$ is the electromagnetic vector, $\boldsymbol{k}^T = 2\pi(u, v, w)/\lambda$ is the wave vector and $\boldsymbol{r}_i = (x_i, y_i, z_i)^T$ is the position of the ith element of the array. (u, v, w) is the unit direction vector of the incident wave on the array antenna, which is usually used in antenna community. Suppose there are N array elements and L subarrays. The amplitude weightings arranged at element level are noted as $\boldsymbol{w}^{ele}$. The phase shift value and the amplitude attenuation of the lth subarray are ψ_l and w_l^{sub}, respectively. Ignoring the polarisation and the time domain feature of the signal, the array output can be

doi: 10.1049/iet-map.2014.0308

expressed as

$$\sum_{l=1}^{L} w_l^{\text{sub}}\, \mathrm{e}^{-\mathrm{j}\psi_l} \sum_{i\in\{n|l_n=l\}} w_i^{\text{ele}}\, \mathrm{e}^{-\mathrm{j}\phi_i}\, \mathrm{e}^{\mathrm{j}\boldsymbol{k}^{\mathrm{T}}\boldsymbol{r}_i} \tag{1}$$

where ϕ_i is the phase shift added at the ith element (if exists) and l_n is the identifier of the subarray which the nth element belongs to. Hence, the set $\{n|l_n=l\}$ are the identifiers of the elements which belong to the lth subarray. This relationship of subarrays and elements can be expressed by the well-known δ function, and then the array output can be rewritten as

$$\begin{aligned}
&\sum_{l=1}^{L} w_l^{\text{sub}}\, \mathrm{e}^{-\mathrm{j}\psi_l} \sum_{i=1}^{N} w_i^{\text{ele}}\, \mathrm{e}^{-\mathrm{j}\phi_i}\, \mathrm{e}^{\mathrm{j}\boldsymbol{k}^{\mathrm{T}}\boldsymbol{r}_i} \delta_{l_i,l} \\
&\quad = \sum_{i=1}^{N} w_i^{\text{ele}}\, \mathrm{e}^{-\mathrm{j}\phi_i}\, \mathrm{e}^{\mathrm{j}\boldsymbol{k}^{\mathrm{T}}\boldsymbol{r}_i} \sum_{l=1}^{L} w_l^{\text{sub}}\, \mathrm{e}^{-\mathrm{j}\psi_l} \delta_{l_i,l} \\
&\quad = \sum_{i=1}^{N} w_i^{\text{ele}} w_{l_i}^{\text{sub}}\, \mathrm{e}^{\mathrm{j}(\boldsymbol{k}^{\mathrm{T}}\boldsymbol{r}_i-\phi_i-\psi_{l_i})}
\end{aligned} \tag{2}$$

where $\delta_{l_i,l} = \begin{cases} 1, l_i=l \\ 0, l_i\neq l \end{cases}$, $w_i^{\text{ele}} w_{l_i}^{\text{sub}}$ is noted by $\tilde{w}_i$, which is named as the equivalent weight of the ith element.

The beam direction is noted by $\boldsymbol{\theta}_{\text{m}}^{\mathrm{T}} = (u_{\text{m}},\ v_{\text{m}},\ w_{\text{m}})$, $\boldsymbol{k}^{\text{m}}$ is $2\pi\theta_{\text{m}}/\lambda$ and $\boldsymbol{k}_{\text{c}}^{\text{m}}$ is $2\pi\theta_{\text{m}}/\lambda_{\text{c}}$, where letters 'm' and 'c' represent the 'main beam' and the 'centre frequency', respectively [Since both θ and $\boldsymbol{k}$ can represent a certain orientation, we use both these two symbols to express the beam direction in this paper. For a planar array, the third component of θ or $\boldsymbol{k}$ can be omitted, for example, using $(u_{\text{m}},\ v_{\text{m}})$ to represent the look direction.]. $\boldsymbol{T}_0$ is a 0-1 matrix, which represents the subarray partition (the $\boldsymbol{T}_0[i,\ j]$ equals to 1 only if the ith element is partitioned into the jth subarray). $\boldsymbol{T}$ is the subarray forming matrix which contains the equivalent weighting at element level, that is, $\boldsymbol{T} = \mathrm{diag}(\tilde{\boldsymbol{w}})\boldsymbol{T}_0$. Theoretically, phase shifters at element level are used to steer the beam peak to an angular position $\boldsymbol{k}_{\text{c}}^{\text{m}}$ by setting the phase-shifting quantities as the phase values of the so-called 'array manifold': $\boldsymbol{a}_{\text{c}}^{\text{m}} = \{\exp(\mathrm{j}\boldsymbol{k}_{\text{c}}^{\text{m}}\cdot\boldsymbol{r}_i)\}_{i=1,\ldots,N}$ [For brevity's sake, the symbol '$\cdot$' is used hereafter to represent the inner product of two vectors (saving many transposes).].

2.2.1 Case I (LFOV): According to Fig. 1*a*, without phase shift at element level, the phase compensating can only be fulfiled at the subarray level. The output of the lth subarray is

$$\begin{aligned}
&\sum_{i=1}^{N} [\delta_{l_i,l}\, \tilde{w}_i\, \mathrm{e}^{\mathrm{j}(\boldsymbol{k}^{\text{m}}\cdot\boldsymbol{r}_i-\psi_l)}] \\
&\quad = \mathrm{e}^{-\mathrm{j}\psi_l} \sum_{i=1}^{N} [\delta_{l_i,l}\, \tilde{w}_i\, \mathrm{e}^{\mathrm{j}\boldsymbol{k}^{\text{m}}\cdot\boldsymbol{r}_i}] \\
&\quad = \mathrm{e}^{-\mathrm{j}\psi_l} \left[\boldsymbol{T}^{\mathrm{H}}\boldsymbol{a}^{\text{m}}\right]_l
\end{aligned} \tag{3}$$

where $[\cdot]_l$ means the lth component of $[\cdot]$. Thus the ideal phase compensating is determined by the array manifold at subarray level, that is, $\boldsymbol{T}^{\mathrm{H}}\boldsymbol{a}^{\text{m}}$. In other words, the ideal quantity of ψ_l is the phase value of the lth component of the vector $\boldsymbol{T}^{\mathrm{H}}\boldsymbol{a}^{\text{m}}$, that is

$$\psi_l = \angle\left[\boldsymbol{T}^{\mathrm{H}}\boldsymbol{a}_0\right]_l \tag{4}$$

where $\angle$ means the taking phase operation.

In practice, there are some non-ideal factors which affect the phase values added at subarray ports. The main reason is that, as a phase shifter, its added phase-shifting values are strictly relevant to the carrier frequency. The subarray phase-shifting values should be obtained based on the frequency selectivity of the phase shifter.

Note that, to steer beam at direction $\boldsymbol{\theta}_{\text{c}}^{\text{m}}$, it is desired that all the terms in (2) are summed up in phase, that is, $\boldsymbol{k}_{\text{c}}^{\text{m}}\cdot\boldsymbol{r}_i - \psi_{l_i} \simeq 0$. Thus according to the theorem in Appendix, we have

$$\begin{aligned}
&\sum_{i=1}^{N} [\delta_{l_i,l}\, \tilde{w}_i\, \mathrm{e}^{\mathrm{j}(\boldsymbol{k}_{\text{c}}^{\text{m}}\cdot\boldsymbol{r}_i-\psi_l)}] \\
&\quad \simeq \left(\sum_{i=1}^{N} \delta_{l_i,l}\, \tilde{w}_i\right) \cdot \exp\left\{ j\frac{\sum_{i=1}^{N} [\delta_{l_i,l}\, \tilde{w}_i\, (\boldsymbol{k}_{\text{c}}^{\text{m}}\cdot\boldsymbol{r}_i - \psi_l)]}{\sum_{i=1}^{N} [\delta_{l_i,l}\, \tilde{w}_i\,]} \right\}
\end{aligned} \tag{5}$$

According to Appendix, as the first-order approximation, the above approximation is quite effective. Since the maximum of the summation in (3) is $\sum_i^N \tilde{w}_i$, we can obtain the reasonable value of ψ_l by simply setting $\sum_{i=1}^{N} [\delta_{l_i,l}\, \tilde{w}_i\, (\boldsymbol{k}_{\text{c}}^{\text{m}}\cdot\boldsymbol{r}_i - \psi_l)] = 0$ in (5). Then

$$\psi_l = \frac{\sum_{i=1}^{N} \delta_{l_i,l}\, \tilde{w}_i\, \boldsymbol{k}_{\text{c}}^{\text{m}}\cdot\boldsymbol{r}_i}{\sum_{i=1}^{N} \delta_{l_i,l}\, \tilde{w}_i} \tag{6}$$

For the theoretic analysis, the calculation of ψ_l mod 2π is omitted. Define $\boldsymbol{\rho}_l$ via

$$\boldsymbol{\rho}_l \triangleq \frac{\sum_{i=1}^{N} \delta_{l_i,l}\, \tilde{w}_i\, \boldsymbol{r}_i}{\sum_{i=1}^{N} \delta_{l_i,l}\, \tilde{w}_i} \tag{7}$$

Thus the phase shift value at subarray level is given by $\boldsymbol{\rho}_l$, that is

$$\psi_l = \boldsymbol{k}_{\text{c}}^{\text{m}}\cdot\boldsymbol{\rho}_l \tag{8}$$

Intuitively, $\boldsymbol{\rho}_l$ can be regarded as a special position of the lth subarray. Specifically, $\boldsymbol{\rho}_l$ can be simply chosen as the position of one of the subarray elements [26]; when the equivalent weighting at element level is uniform, $\boldsymbol{\rho}_l$ is just the geometric centre of the lth subarray; when $w_l^{\text{sub}} = 1$, for $\forall l$, $\boldsymbol{\rho}_l$ is the subarray centre given in [33]. In (7), both the element weighting and subarray weighting are considered, so $\boldsymbol{\rho}_l$ is called as the generalised subarray phase centre (GSPC) in this paper.

2.2.2 Case II (WBWS): When the phase shifters are used at the element level, the phase-shifting value provided by the ith element can compensate the phase delay aroused by the plane wave at the centre frequency impinging on the array from a given direction. Using the above notations, we can parameterise the incident wave by $\boldsymbol{k}_{\text{c}}^{\text{m}}$. Correspondingly, the phase-shifting value provided by the ith element is

$$\phi_i = \boldsymbol{k}_{\text{c}}^{\text{m}}\cdot\boldsymbol{r}_i \tag{9}$$

The time delays at subarray ports compensate the phase difference of the other frequency wave at the given

direction ($\boldsymbol{k}^{\mathrm{m}}$). Thus, similarly to (5), we have

$$\sum_{i=1}^{N}\left[\delta_{l_i,l}\,\tilde{w}_i\,(\boldsymbol{k}^{\mathrm{m}}\cdot\boldsymbol{r}_i-\overbrace{\boldsymbol{k}_{\mathrm{c}}^{\mathrm{m}}\cdot\boldsymbol{r}_i}^{\phi_i}-\psi_l)\right]=0 \tag{10}$$

Therefore

$$\psi_l=(\boldsymbol{k}^{\mathrm{m}}-\boldsymbol{k}_{\mathrm{c}}^{\mathrm{m}})\cdot\boldsymbol{\rho}_l \tag{11}$$

A more general expression of the ideal quantity of ψ_l similar to (4) is

$$\psi_l=\angle\left[\boldsymbol{T}^{\mathrm{H}}\mathrm{diag}(\boldsymbol{a}_{\mathrm{c}}^{\mathrm{m}})^{*}\boldsymbol{a}^{\mathrm{m}}\right]_l \tag{12}$$

If both the phase-shifting values and the amplitude values are included in the subarray forming matrix $\boldsymbol{T}$, that is

$$\boldsymbol{T}=\mathrm{diag}(\boldsymbol{a}_{\mathrm{c}}^{\mathrm{m}})\mathrm{diag}(\tilde{\boldsymbol{w}})\boldsymbol{T}_0 \tag{13}$$

then, both the right parts of (4) and (12) can be written as $\angle[\boldsymbol{T}^{\mathrm{H}}\boldsymbol{a}^{\mathrm{m}}]_l$, where $\boldsymbol{T}^{\mathrm{H}}\boldsymbol{a}^{\mathrm{m}}$ is called subarray manifold in the literature.

Above all, the weighting methods for LFOV and WBWS for array antennas with arbitrary subarray partitioning are

$$\begin{cases}\phi_i=0,\ \psi_l=\boldsymbol{k}_{\mathrm{c}}^{\mathrm{m}}\cdot\boldsymbol{\rho}_l & \text{(LFOV)}\\ \phi_i=\boldsymbol{k}_{\mathrm{c}}^{\mathrm{m}}\cdot\boldsymbol{r}_i,\ \psi_l=(\boldsymbol{k}^{\mathrm{m}}-\boldsymbol{k}_{\mathrm{c}}^{\mathrm{m}})\cdot\boldsymbol{\rho}_l & \text{(WBWS)}\end{cases} \tag{14}$$

where $i=1,\ \ldots,\ N$ and $l=1,\ \ldots,\ L$ are the indexes of all elements and subarrays, respectively. The ideal phase compensating at subarray level is determined by the subarray manifold $\boldsymbol{T}^{\mathrm{H}}\boldsymbol{a}^{\mathrm{m}}$, where $\boldsymbol{T}$ is the subarray forming matrix which contains the amplitude weighting and phase-shifting weighting (if exist). It is worth mentioning that after the digitalisation at subarray level, there are fruitful processing technologies could be applied which are not limited to the LFOV or WBWS. The above analysis is limited to the typical applications such as LFOV and WBWS, which are sufficient for most designs.

The subarray partitioning method, parameterised by the subarray forming matrix $\boldsymbol{T}$, is arbitrary (i.e. partitioning could be overlapped or non-overlapped, regular or irregular etc.). Although there is only one layer of the subarray architecture in the above analyses, the ideas apply to multi-layer arrays as well.

2.3 Experimental tests

In the following, we take the LFOV application as an example to illustrate the effects of the above weighting methods. Consider a linear array with 32 omnidirectional elements. The array has a 35 dB Taylor taper and the inter-element space is $\lambda/2$. Fig. 2*a* shows the scanned pattern of the array with two different non-overlapped partitioning strategies, where the regular partition is (4, 4, 4, 4, 4, 4, 4, 4), and the irregular one is (7, 4, 2, 3, 3, 2, 4, 7). The offset beam is steered to 8.63° (or $u_{\mathrm{m}}=0.15$, $v_{\mathrm{m}}=0$).

On the basis of the above analyses, the phase shift values are determined by the first equation in (14). The number of control ports of the two arrays is equal. The only factor, which causes the differences between their patterns, is the subarray partitioning strategy. Further discussion about the

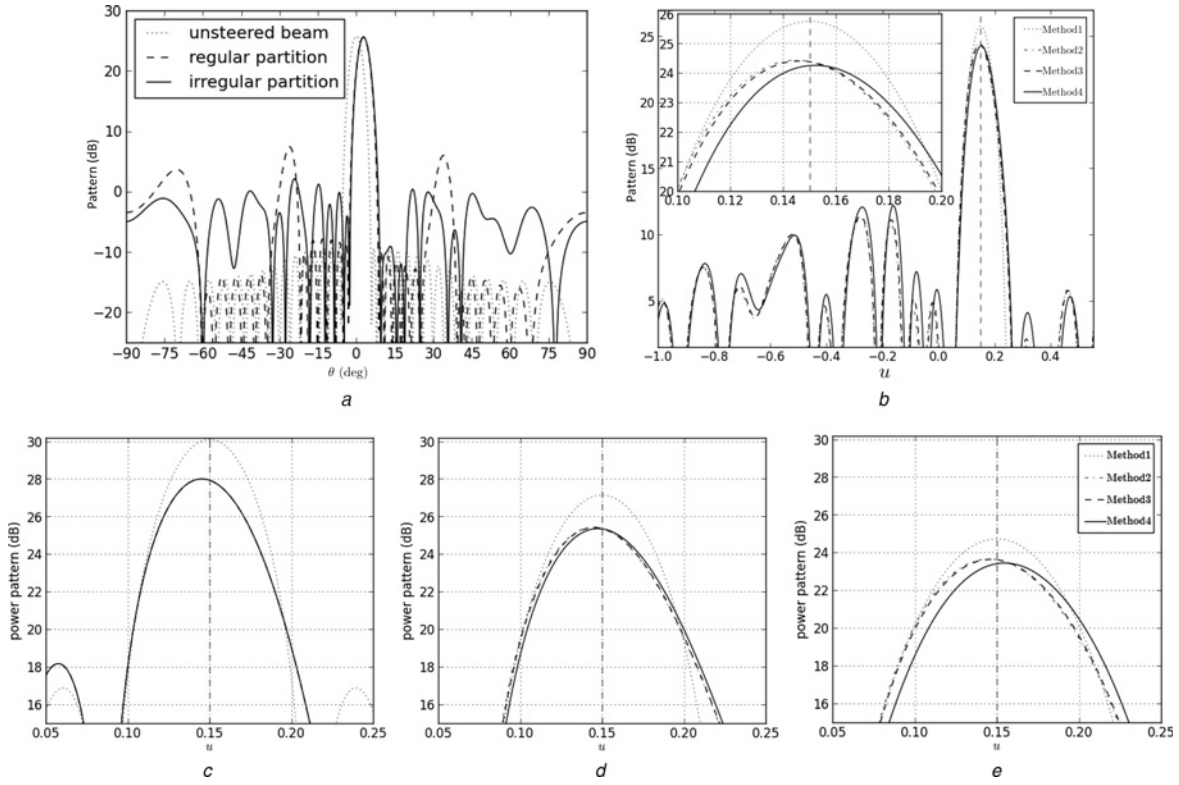

Fig. 2 *Examples of the steered and un-steered beams with different phase controlling methods and weighting tapers*

a 35 dB Taylor weighting
b Uniformly excitation
c 25 dB Taylor weighting
d 45 dB Taylor weighting

doi: 10.1049/iet-map.2014.0308

irregular subarray partition will be given in the next section. To show the predominance of the phase weighting method given by the GSPC, four different weighting methods are compared:

- *Method 1:* All phase weights are controlled at the element level, which is equivalent to that the subarrays does not exist. By adjusting the phase shifters at every element, this method can compensate the full array manifold $\boldsymbol{a}_{\mathrm{c}}^{\mathrm{m}}$.
- *Method 2:* The ideal phase control method at subarray level (shown by (3)).
- *Method 3:* Phase-shifting values at subarray level are determined by the GSPC as shown in (6), which has been used in Fig. 2*a*.
- *Method 4:* Phase-shifting values at subarray level are calculated by (8), whereas the $\boldsymbol{\rho}_l$ is the geometric centre of the lth subarray.

Fig. 2*b* shows the scanned patterns by four-phase control methods. The vertical dashed line gives the steered direction, that is, $u_{\mathrm{m}} = 0.15$. As shown in Fig. 2*b*, the Method 2 and Method 3 have a relatively small amount of directivity loss and low side lobe level. Since the phase-shifting values which are calculated according to GSPC are very close to the ideal values, the differences between the patterns given by Method 2 and Method 3 are relatively few.

Further comparisons of different phase control methods are shown in Figs. 2*c*–*e*. Fig. 2*c* shows the patterns of the array with uniformed excitation at element level. In this case, there is no difference between Methods 2 and 4. This is because that the GSPCs are the same as the geometric centres of subarrays. In Figs. 2*d* and *e*, patterns for array with 25 and 45 dB Taylor weightings are illustrated, respectively. According to the results in Fig. 2, one can find that the beam-pointing direction for Method 3 does not change with the amplitude weighting at element level. This is a good characteristic. Although the shifting of the beam-pointing direction corresponding to the Method 4 is not desired, the beam-pointing error can be eliminated by applying a precomputed correction factor.

Considering the advantage of the Method 3, we suggest to use this method to design the phase-shifting values in practice. The phase control method by the GSPC will be used as the default method in the following analysis unless with special instruction.

3 Beamforming properties for subarrayed antennas

3.1 Antenna pattern

Although the subarray configuration and the weighting strategy given, the antenna pattern for an array with omnidirectional elements can be calculated via

$$F(\boldsymbol{k}) = (\boldsymbol{w}^{\mathrm{sub}})^{\mathrm{H}}(\boldsymbol{T}^{\mathrm{H}}\boldsymbol{a}) \tag{15}$$

where $\boldsymbol{a} = \{\exp(\mathrm{j}\boldsymbol{k}\cdot\boldsymbol{r}_i)\}_{i=1,\ldots,N}$ is the array manifold – the complete knowledge of the array outputs for a plane wave impinging on the array. Without any superscript and subscript, $\boldsymbol{k}$ represents the monochromatic plane electromagnetic wave with any frequencies and incident direction.

Theoretically, beam direction can be adjusted at element or subarray level. The phase steering vector corresponding to the direction adjusting at element level is noted as $\boldsymbol{a}^{\mathrm{ele}}(\boldsymbol{k}_1) = \{\exp(\mathrm{j}\boldsymbol{k}_1\cdot\boldsymbol{r}_i)\}_{i=1,\ldots,N}$. Then, the array manifold at subarray level is

$$\{\mathrm{diag}[\boldsymbol{w}^{\mathrm{ele}}]\mathrm{diag}[\boldsymbol{a}^{\mathrm{ele}}(\boldsymbol{k}_1)]\boldsymbol{T}_0\}^{\mathrm{H}}\boldsymbol{a} = \{\mathrm{diag}[\boldsymbol{w}^{\mathrm{ele}}\odot\boldsymbol{a}^{\mathrm{ele}}(\boldsymbol{k}_1)]\boldsymbol{T}_0\}^{\mathrm{H}}\boldsymbol{a} \tag{16}$$

where $\odot$ means the Hadamard product, that is, the element-wise multiply. The amplitude and phase weights at subarray level can be written as $\boldsymbol{w}^{\mathrm{sub}}\odot\boldsymbol{a}^{\mathrm{sub}}(\boldsymbol{k}_2)$. The phase weighting of beam scanning at subarray level is determined by the GSPC, thus

$$[\boldsymbol{w}^{\mathrm{sub}}\odot\boldsymbol{a}^{\mathrm{sub}}(\boldsymbol{k}_2)]_l = w_l^{\mathrm{sub}}\exp(\mathrm{j}\boldsymbol{k}_2\cdot\boldsymbol{\rho}_l) \tag{17}$$

Therefore after two stages adjusting (element level and subarray level), the antenna pattern can be expressed as

$$F(\boldsymbol{k}) = [\boldsymbol{w}^{\mathrm{sub}}\odot\boldsymbol{a}^{\mathrm{sub}}(\boldsymbol{k}_2)]^{\mathrm{H}}\{\mathrm{diag}[\boldsymbol{w}^{\mathrm{ele}}\odot\boldsymbol{a}^{\mathrm{ele}}(\boldsymbol{k}_1)]\boldsymbol{T}_0\}^{\mathrm{H}}\boldsymbol{a} \tag{18}$$

If required, one can extend the above derivations to the subarrayed antennas with multiple layers. With some shorthand notations, the antenna pattern for an antenna with multi-layer subarrays ($M-1$ layers in total) is

$$\begin{aligned} F(\boldsymbol{k}) = {} & (\boldsymbol{w}_M\odot\boldsymbol{a}_M)^{\mathrm{H}} \\ & \times[\mathrm{diag}(\boldsymbol{w}_{M-1}\odot\boldsymbol{a}_{M-1})\boldsymbol{T}_{M-2}]^{\mathrm{H}} \\ & \vdots \\ & \times[\mathrm{diag}(\boldsymbol{w}_1\odot\boldsymbol{a}_1)\boldsymbol{T}_0]^{\mathrm{H}}\boldsymbol{a} \end{aligned} \tag{19}$$

where the numbered subscripts are used to distinguish the subarray processing between different layers. $\boldsymbol{w}_m$ and $\boldsymbol{a}_m$ are the $m-1$th subarray's amplitude weights and phase-shifting weights, respectively ($\boldsymbol{w}_1$ and $\boldsymbol{a}_1$ are arranged at element level). The $\boldsymbol{T}_{m-1}$ is the subarray partitioning matrix of the mth layer subarray. The steering vector $\boldsymbol{k}_m$ of the $m-1$th layer subarray is implied in $\boldsymbol{a}_m$, while the symbol $\boldsymbol{a}$, without any subscripts, is corresponding to the monochromatic plane electromagnetic wave parameterised by $\boldsymbol{k}$. If we are only interested in the beam scanning, we can display these beam steering vectors in pattern function, that is, $F(\boldsymbol{k}, \boldsymbol{k}_1, \boldsymbol{k}_2, \ldots, \boldsymbol{k}_M)$.

Note that there no constraints on subarray configuration in (19). Thus, this antenna pattern calculation method is applicable for any subarray architectures. Besides, conventionally, only the last stage is digital, but in principle analogue-to-digital conversion can take place between any two processing layers or not at all. For antennas with special subarray architectures, the calculation in (19) can be simplified into particular forms, such as the analysis for the overlapped multi-layer subarray shown in [18]. In fact, the key to do the further simplification is the regularity of the architecture, for example, the regularly contiguous subarrays or the periodically overlapped subarrays. This paper is limited to antennas with irregularly subarray partitioning, and we focus on the single-layer subarray architecture.

As a single-layer architecture, the beam scanning can be realised by adjusting $\boldsymbol{k}_1$ and $\boldsymbol{k}_2$. In summary, the antenna

patterns for LFOV and WBWS are $F(\boldsymbol{k},\ \boldsymbol{k}_1 = \boldsymbol{0},\ \boldsymbol{k}_2 = \boldsymbol{k}_{\mathrm{c}}^{\mathrm{m}})$ and $F(\boldsymbol{k},\ \boldsymbol{k}_1 = \boldsymbol{k}_{\mathrm{c}}^{\mathrm{m}},\ \boldsymbol{k}_2 = \boldsymbol{k}^{\mathrm{m}})$, respectively. Specific analysis for the LFOV is developed as follows.

The ith element pattern is noted as $f_i^{\mathrm{e}(\boldsymbol{k})}$, then one can write the pattern by superposition

$$\begin{aligned} F(\boldsymbol{k}) &= \sum_{i=1}^{N} \tilde{\boldsymbol{w}}_i \, \mathrm{e}^{\mathrm{j}(\boldsymbol{k}\cdot\boldsymbol{r}_i - \boldsymbol{k}_{\mathrm{c}}^m\cdot\boldsymbol{\rho}_{l_i})} f_i^{\mathrm{e}}(\boldsymbol{k}) \\ &= \sum_{i=1}^{N} \tilde{\boldsymbol{w}}_i \, \mathrm{e}^{\mathrm{j}(\boldsymbol{k}\cdot\boldsymbol{\rho}_{l_i} - \boldsymbol{k}_{\mathrm{c}}^m\cdot\boldsymbol{\rho}_{l_i})} \, \mathrm{e}^{\mathrm{j}(\boldsymbol{k}\cdot\boldsymbol{r}_i - \boldsymbol{k}\cdot\boldsymbol{\rho}_{l_i})} f_i^{\mathrm{e}}(\boldsymbol{k}) \\ &= \sum_{l=1}^{L} [\mathrm{e}^{\mathrm{j}(\boldsymbol{k}-\boldsymbol{k}_{\mathrm{c}}^m)\cdot\boldsymbol{\rho}_l} \underbrace{\sum_{i=1}^{N} \delta(l_i,\ l)\tilde{\boldsymbol{w}}_i \, \mathrm{e}^{\mathrm{j}(\boldsymbol{k}\cdot\boldsymbol{r}_i - \boldsymbol{k}\cdot\boldsymbol{\rho}_l)} f_i^{e}(\boldsymbol{k})}_{f_l^{\mathrm{s}}(\boldsymbol{k})}] \\ &= \sum_{l=1}^{L} \mathrm{e}^{\mathrm{j}(\boldsymbol{k}-\boldsymbol{k}_{\mathrm{c}}^m)\cdot\boldsymbol{\rho}_l} f_l^{\mathrm{s}}(\boldsymbol{k}) \end{aligned} \tag{20}$$

where $f_l^{\mathrm{s}}(\boldsymbol{k})$ is the lth subarrays pattern and $\boldsymbol{k}_{\mathrm{c}}^{\mathrm{m}}$ is the direction the array electronically scanned to.

According to the concept of the GSPC, subarray array factor (SAF) is defined as

$$\mathrm{SAF}(\boldsymbol{k},\ \boldsymbol{k}_{\mathrm{c}}^m) = \sum_{l=1}^{L} \mathrm{e}^{\mathrm{j}(\boldsymbol{k}-\boldsymbol{k}_{\mathrm{c}}^m)\cdot\boldsymbol{\rho}_l} \tag{21}$$

Treating the GSPC as phase centres of omnidirectional 'super-array' elements [33], one can find that the SAF is just the antenna pattern of the super-array.

Generally, each subarray has a relatively broad pattern. If the scanning region is relatively small, it is acceptable to neglect the differences between subarrays' patterns. Therefore $f_l^{\mathrm{s}}(\boldsymbol{k}) \simeq f^{\mathrm{s}}(\boldsymbol{k}),\ \forall l$. Thus, in a small scanning coverage, the antenna pattern can be approximated as

$$F(\boldsymbol{k},\ \boldsymbol{k}_{\mathrm{c}}^m) \simeq \mathrm{SAF}(\boldsymbol{k},\ \boldsymbol{k}_{\mathrm{c}}^m) f^{\mathrm{s}}(\boldsymbol{k}) \tag{22}$$

Thus, one can think of the pattern as being the product of the average subarray pattern and SAF. This conclusion can be thought as the generalisation the ordinary product principle of array antennas. The arithmetic mean of $f_l^{\mathrm{s}}(\boldsymbol{k})$ is a simple way to estimate $f^{\mathrm{s}}(\boldsymbol{k})$, that is

$$\begin{aligned} f^{\mathrm{s}}(\boldsymbol{k}) &= \frac{1}{L}\sum_{l=1}^{L} f_l^{\mathrm{s}}(\boldsymbol{k}) \\ &= \frac{1}{L}\sum_{l=1}^{L}\sum_{i=1}^{N} \delta_{l_i,l}\tilde{\boldsymbol{w}}_i \, \mathrm{e}^{\mathrm{j}(\boldsymbol{k}\cdot\boldsymbol{r}_i - \boldsymbol{k}\cdot\boldsymbol{\rho}_l)} f_i^{e}(\boldsymbol{k}) \end{aligned} \tag{23}$$

Equation (22) illustrates a simple method to assess the performance of the beam pattern. Specifically, the effect of grating-lobe-level can be described by SAF; the loss of the offset beam can be calculated by the average subarray pattern.

3.2 Numerical results

To show the performance of the proposed analysis method, we design reasonable subarray configurations which are shown in Fig. 3. Fig. 3*b* shows an exact partition of an array with 64×32 elements by L-octomino-shaped subarrays. For the sake of comparison, an ordinary design of subarrays is shown in Fig. 3*a*, in which the individual

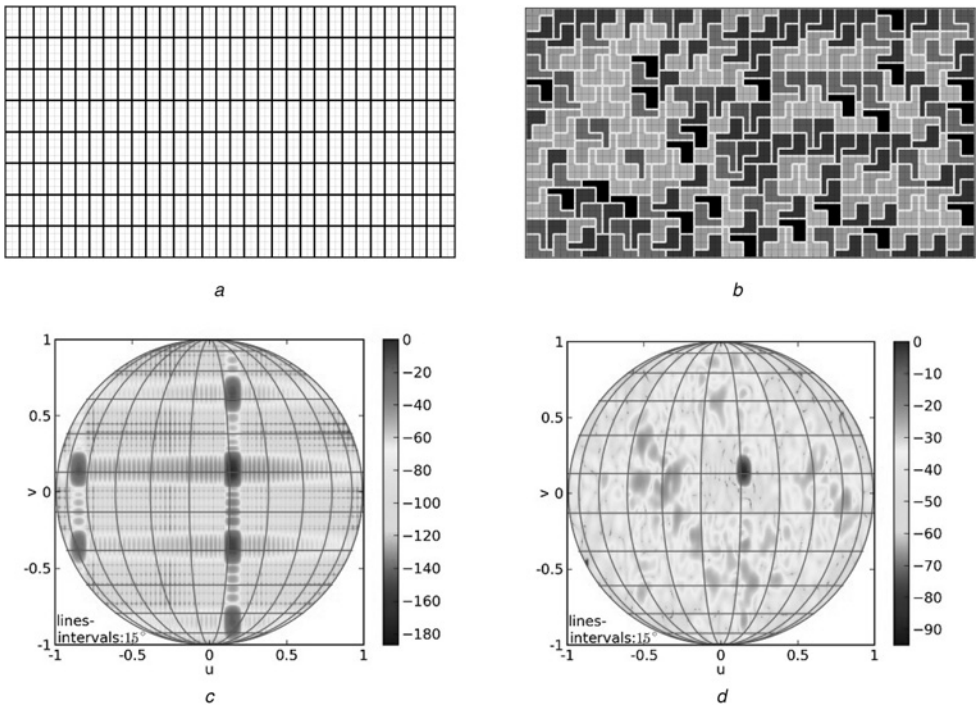

Fig. 3 *Two arrays with different partitioning strategies and their patterns*

a First array
b Second array
c Pattern of the first array
d Pattern of the second array

IET Microw. Antennas Propag., 2015, Vol. 9, Iss. 4, pp. 369–379
doi: 10.1049/iet-map.2014.0308

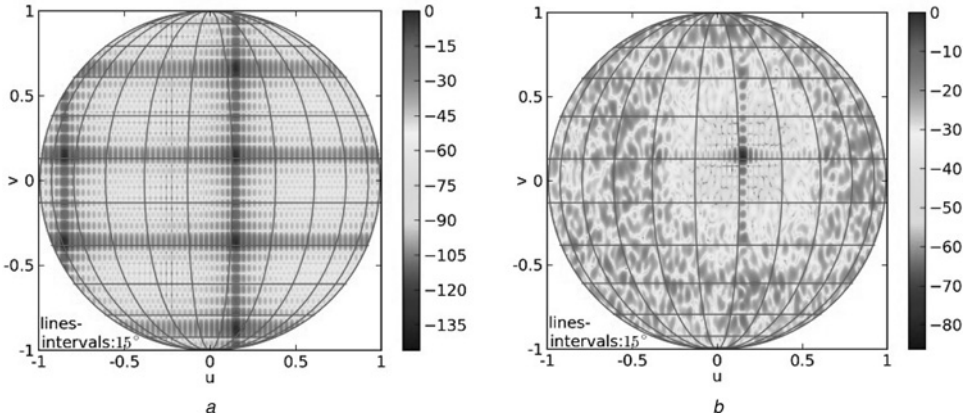

Fig. 4 *SAF for two arrays*

a SAF of the first array
b SAF of the second array

elements are grouped into 256 rectangular subarrays (two elements in the elevation plane and four in the azimuth plane). With 40 dB Taylor taper arranging at the array face, the inter-element space is $\lambda/2$. The element pattern is assumed to be $\cos\theta$, while θ is the angle of beam deflection from the boresight. Consider the LFOV application, thus the phase shifters are installed at the subarray ports not at the element level.

We set the beam-pointing direction is $(u_m, v_m) = (0.15, 0.15)$. Figs. 3*c* and *d* show the normalised patterns of the above described arrays. The pattern for the ordinary designed array (Fig. 3*a*) has five quantisation lobes. The

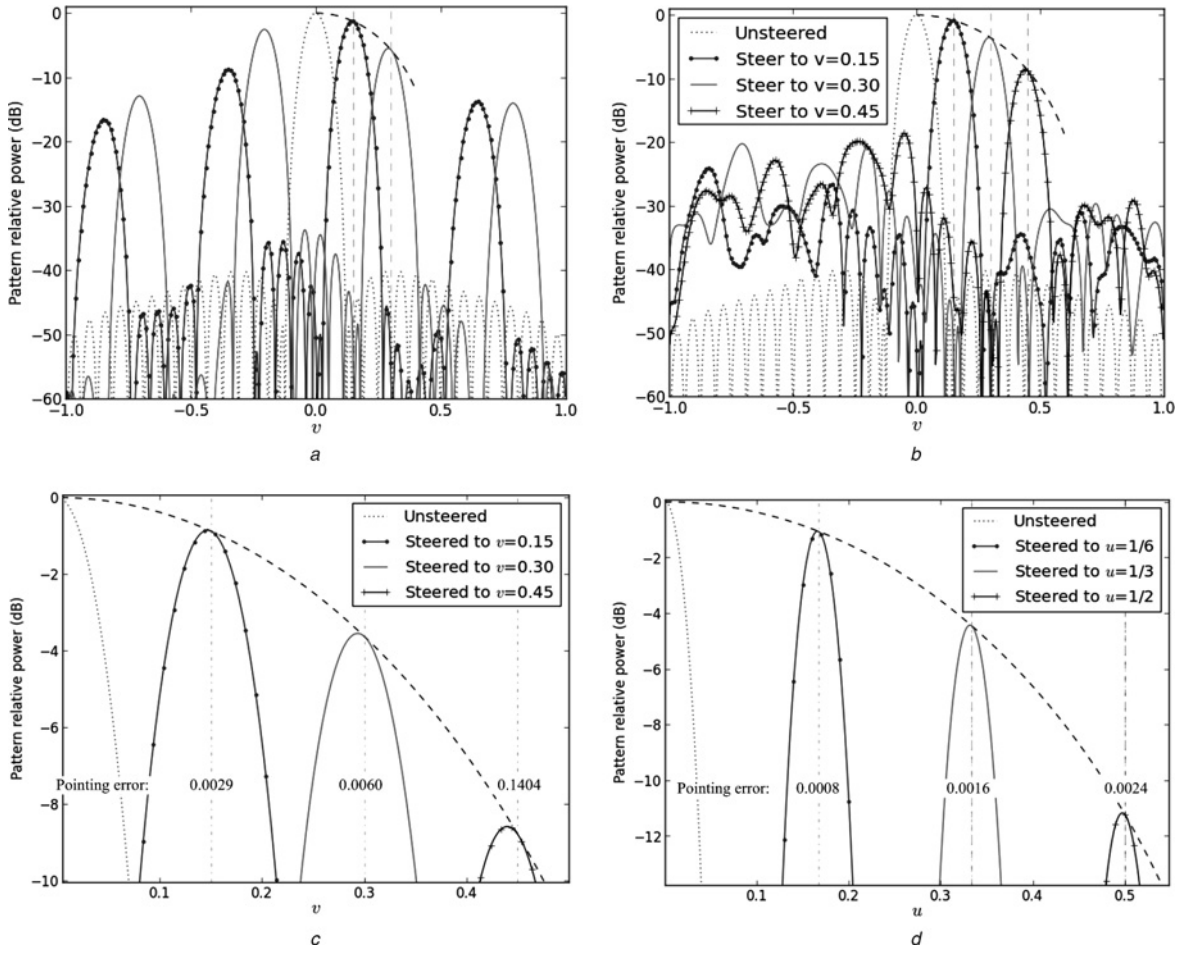

Fig. 5 *Scanning patterns of two arrays*

a Scanning pattern of the first array
b Scanning pattern of the second array
c Scanning in elevation (the second array)
d Scanning in azimuth (the second array)

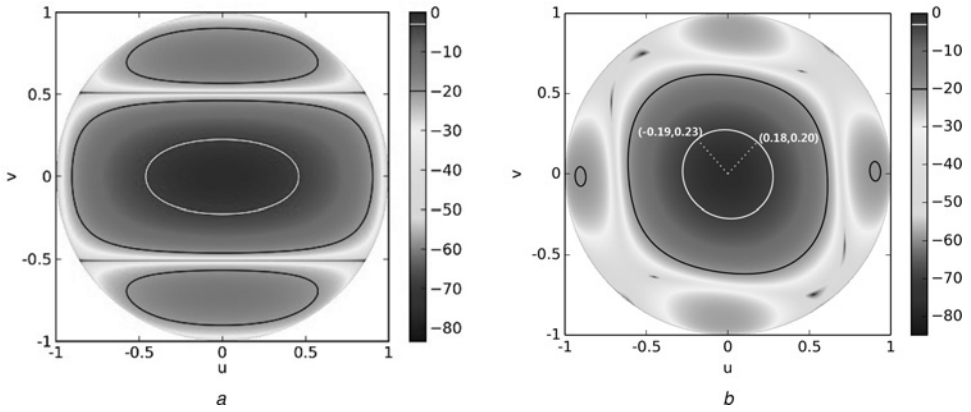

Fig. 6 *Average subarray pattern*

a Average pattern of the first array
b Average pattern of the second array

largest one of these lobes is −7.5 dB. Although the pattern of the array with irregular subarrays (Fig. 3*b*) has no quantisation lobes and the side lobes are lower than −20 dB.

By applying the concept of the approximate relation given in (22), it is convenient to obtain the useful description and conclusion of the beamforming properties. The relative results for the above rectangular arrays are shown as follows.

(1) *Grating lobes:* According to (22), the emergence of grating lobes can be ascribed to the periodically distribution of the GSPCs. Fig. 4 shows the comparison of the SAF different arrays, which are calculated according to (21). For the regular partitioning, the distribution of GSPCs has a strong periodicity (although the tapering weights at element level can weaken the periodicity to some extent), which results in the very high quantisation lobes in the total pattern (Fig. 4*a*). Although the irregular partitioning strongly distorts the periodicity of the GSPCs. Thus, the grating lobes of SAF are migrated considerably (Fig. 4*b*).

(2) *Gain loss:* According to the approximate product relation given by (22), the gain loss of the offset beam can be estimated by the average subarray pattern. Figs. 5*a* and *b* show the patterns for different steered elevations (with u_m fixed at zero). The black dashed curve is the average subarray pattern calculated by (23), and the scanned patterns pointing at different steered directions are calculated by (20). Fig. 5*c* shows the partial enlarged details of Fig. 5*b*; Fig. 5*d* shows the similar results for the second antenna scanning along the azimuth direction. It is shown that the changing of the gain of the main lobe is nearly in accordance with the changing of the average subarray pattern.

Besides, the approximate error of (22) becomes large far away from the beam-pointing direction. Thus, the sidelobe level cannot be estimated by the average subarray pattern. However, for the high quantisation lobes, the average subarray pattern also provides good estimation for their levels (as shown in Fig. 5*a*).

Interestingly, the maximum of the total pattern is not always at the $\boldsymbol{k}_c^m$ which is set in advance (shown in (20)). The pointing errors for different scanning are illustrated in Figs. 5*c* and *d* at the beam-pointing locations. The main reason for the existence of pointing error is that the subarray pattern is not omnidirectional.

4 Elaborate subarray partitioning

We now turn to the question of how to optimise the subarray configuration according to the beamforming properties.

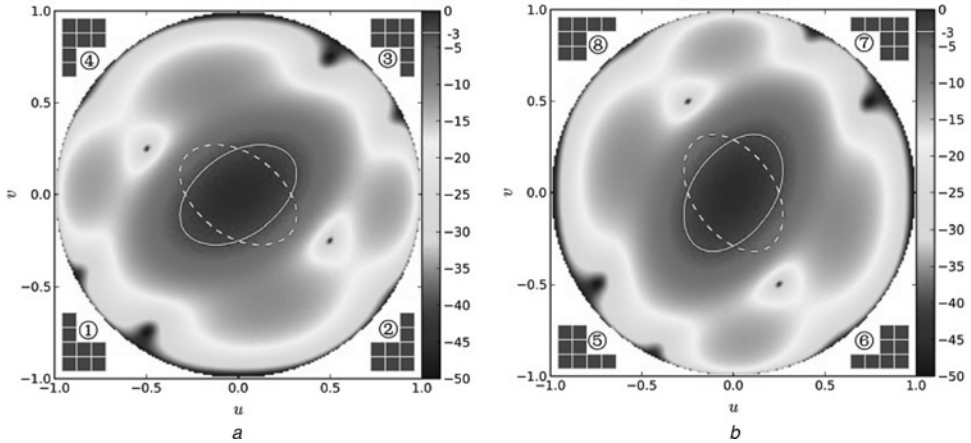

Fig. 7 *Patterns of subarrays with different shapes*

a Subarrays ①–④
b Subarrays ⑤–⑧

doi: 10.1049/iet-map.2014.0308

Table 1 Number of subarrays with different shapes

Subarray	Number
①	30
②	40
③	23
④	39
⑤	32
⑥	34
⑦	22
⑧	36
① + ③	53
② + ④	79
⑤ + ⑦	54
⑦ + ⑧	70

Considerations for the above rectangular array with polyomino-shaped subarrays are shown as follows.

4.1 Subarray configuration and angular coverage

It has been recognised that the average subarray pattern gives the gain loss of the scanned beam. Thus, considering the requirement of the antenna gain, an upper bound for LFOV scanning can be simply determined by the half-power region of the average subarray pattern. In this paper, using the average subarray pattern, we can obtain an estimation of the bound (angular field of view) for LFOV scanning.

Fig. 6 shows the average subarray pattern for the above two arrays in the entire visible region. The contour levels at decibel values −3 and −20 dB are illustrated with different colour lines. The region of the half-power beam of the first array is larger than the second one. However, it does not mean the first array has a larger angular field of view, because the grating-lobes are not negligible for the first array. Anyhow, one can use the average subarray pattern to estimate the gain loss of the beam at the pointing direction. As an array partitioned by irregular-shaped subarrays, the average subarray pattern is a good estimation for the angular coverage.

In fact, the shape of subarray is also the key factor which impacts the average subarray pattern. To illustrate this point, Fig. 7 shows the patterns of the eight different subarrays which are indexed by ①–⑧. Without considering the tapering effect in these subarrays, whole patterns for the subarrays ①, ③, ⑤ and ⑦ are completely shown in Fig. 7. Subarrays ① and ③ have the same pattern which is shown in Fig. 7*a*, and the similar result for subarrays ⑤ and ⑦ is shown in Fig. 7*b*. Considering the symmetry, we only show the half-power beam region of the pattern for subarrays ② and ④ by a white dashed line in Fig. 7*a*, and the similar result for subarrays ⑥ and ⑧ is shown in Fig. 7*b*. The careful readers can find that the patterns shown in Fig. 7*b* can be obtained by those patterns shown in Fig. 7*a* with 90° rotation.

The number of subarrays with different shapes is listed in Table 1. Obviously, subarrays ②, ④, ⑥ and ⑧ are more than the others. From Figs. 6 and 7, we know that the difference between the numbers of different subarray shapes is the primary cause for the squint of the average subarray pattern. Take the 3 dB contour line in Fig. 6*b* as an example to describe the squint of pattern, the farthest points away from

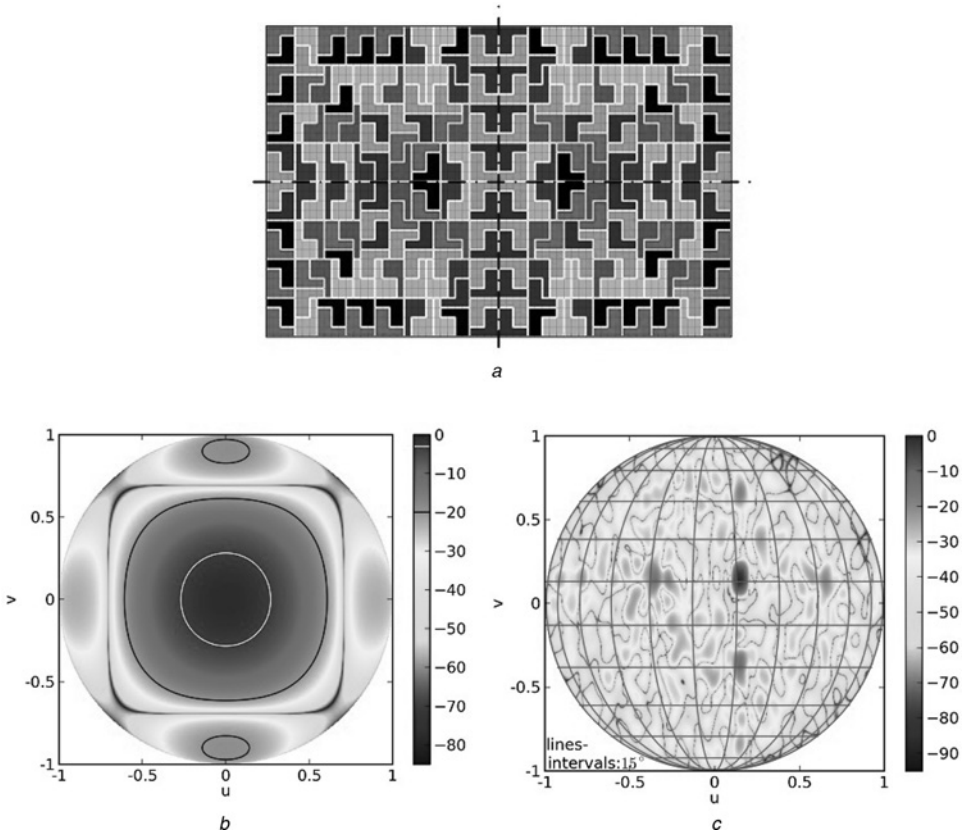

Fig. 8 *Array with symmetric subarray configuration and special control of subarray number and its patterns*

a Array architecture
b Average subarray pattern
c Steered antenna pattern

(0,0) in the first quadrant is (0.18,0.20) (and the corresponding point in the second quadrant is (−0.19,0.23)). If we use the 3 dB contour line to assess angular coverage of the antenna, which means that the gain loss is about 3 dB at the maximum scanning location, one can obtain the maximum offset angle in the first and third quadrants is about 15.6°, while is 17.4° in the second and fourth quadrants.

4.2 Optimisation example of subarray partitioning

The average subarray pattern determines a basic angular field of view, and this field can never be adjusted in the post-processing. Therefore, to design a desired angular coverage region, it is necessary to optimise the design of each subarray.

According to the analysis above, the angular coverage can be adjusted by designing the average subarray pattern. We give a simple example here. Making the number of subarrays ① and ③ ($N_1 + N_3$) equals to the subarrays ② and ⑥ ($N_2 + N_4$), meanwhile, the number of subarrays ⑤ and ⑦ ($N_5 + N_7$) equals to the subarrays ⑥ and ⑧ ($N_6 + N_8$), one can obtain a symmetrical average subarray pattern. In another words, there is no squint of the angular coverage as shown in Fig. 6*b* by this design. Note the existence of the cross-polarisation with the non-ideal factors. It is suggested to design an array with symmetry. In fact, the symmetry of the array is important in determining the characteristics of the co-polarisation and cross-polarisation array factors. Inspired by the research on the control of polarisation in [34–36], we give a special symmetric subarray configuration in Fig. 8*a*. Thanks to the symmetric architecture, the lower cross-polarisation than the design given in Fig. 3*b* can be obtained. The number of subarrays satisfies: $N_1 + N_3 = N_2 + N_4 = 80$ and $N_5 + N_7 = N_6 + N_8 = 48$. How much improvement could be obtained by the symmetric design primarily depends on the type of array element and the feeding circuitry. Owing to the page limitation, the further discussion is not given in this paper.

Fig. 8*b* shows the average pattern of this array with symmetric subarray configuration. As shown in Fig. 8*b*, there is no squint of the average pattern. The steered pattern is shown in Fig. 8*c*, while the beam direction is $(u_m, v_m) = (0.15, 0.15)$.

5 Conclusion

This paper investigated the beamforming technologies for the subarrayed array antennas. The uniform model of the beamforming for arrays with arbitrary subarray partition was established, and the architecture with irregular-shaped subarrays was treated as the key point in this paper. The widely used beamforming technologies, such as LFOV, WBWS and MSB, were summarised and analysed. The approximate product principle of antenna pattern was presented to describe the beamforming properties of the irregularly subarrayed antennas. The following characteristics can be used for the subarray analysis and design: (i) both the mechanism of the tapering weights and the irregularly subarray partitioning on the migrating of grating lobes can be explained by applying the SAF, or equivalently, the distribution of the GSPCs; (ii) the average subarray pattern can be used to estimate the gain of the main lobe as well and the quantisation lobes; and (iii) the shapes and locations of subarrays directly impact the effects of grating-lobe. One can use SAF to obtain the number and location of the quantisation lobe.

A simple example illustrated the design discipline for an LFOV array with polyomino-shaped subarrays.

These new results of the irregular-shaped subarrays are useful for the analysis and further studies on the subarray technique.

6 Acknowledgment

This work was supported in part by the National Natural Science Foundation of China (NSFC) under grant no. 41301490 and 61471372.

7 References

1 Nickel, U.R.: 'Subarray configurations for digital beamforming with low sidelobes and adaptive interference suppression'. IEEE Int. Radar Conf., 1995, pp. 714–719
2 Nickel, U.R.: 'Overview of generalized monopulse estimation', *IEEE Aerosp. Electron. Syst. Mag.*, 2006, **21**, (6), pp. 27–56
3 Mailloux, R.J.: 'Subarray technology for large scanning arrays'. EuCAP, The Second European Conf., IET, 2007, pp. 1–6
4 Brookner, E.: 'Phased-array and radar astounding breakthroughs – an update'. Int. Radar Conf., IEEE, 2008, pp. 1–6
5 Rocca, P., Manica, L., Stringari, F., *et al.*: 'Ant colony optimisation for tree-searching-based synthesis of monopulse array antenna', *IET Electron. Lett.*, 2008, **44**, (13), pp. 783–785
6 Melvin, W.L., Scheer, J.A.: 'Principles of modern radar: advanced techniques' (SciTech Pub., Edison, NJ, 2013)
7 Xiong, Z.Y., Xu, Z.H., Chen, S.W., *et al.*: 'Subarray partition in array antenna based on the algorithm X', *IEEE Antennas Wirel. Propag. Lett.*, 2013, **12**, pp. 906–909
8 Isernia, T., DUrso, M., Bucci, O.: 'A simple idea for an effective sub-arraying of large planar sources', *IEEE Antennas Wirel. Propag. Lett.*, 2009, **8**, pp. 169–172
9 Rocca, P., Manica, L., Martini, A., *et al.*: 'Synthesis of large monopulse linear arrays through a tree-based optimal excitations matching', *IEEE Antennas Wirel. Propag. Lett.*, 2007, **6**, pp. 436–439
10 Manica, L., Rocca, P., Oliveri, G., *et al.*: 'Synthesis of multi-beam sub-arrayed antennas through an excitation matching strategy', *IEEE Trans. Antennas Propag.*, 2011, **59**, (2), pp. 482–492
11 Xiong, Z.Y., Xu, Z.H., Zhang, L., *et al.*: 'Cluster analysis for the synthesis of subarrayed monopulse antennas', *IEEE Trans. Antennas Propag.*, 2014, **62**, (4), pp. 1738–1749
12 Mailloux, R.J.: 'Phased array antenna handbook' (Artech House Boston, MA, 2005)
13 Brockett, T.J., Rahmat-Samii, Y.: 'Subarray design diagnostics for the suppression of undesirable grating lobes', *IEEE Trans. Antennas Propag.*, 2012, **60**, (3), pp. 1373–1380
14 Mailloux, R.J.: 'Electronically scanned arrays', *Synth. Lect. Antennas*, 2007, **2**, (1), pp. 1–82
15 Mailloux, R.J.: 'A low-sidelobe partially overlapped constrained feed network for time-delayed subarrays', *IEEE Trans. Antennas Propag.*, 2001, **49**, (2), pp. 280–291
16 Skobelev, S.P.: 'Phased array antennas with optimized element patterns' (Artech House, Norwood, MA, 2011)
17 Mailloux, R.J., Santarelli, S., Roberts, T.: 'Wideband arrays using irregular (polyomino) shaped subarrays', *IET Electron. Lett.*, 2006, **42**, (18), pp. 1019–1020
18 Coleman, J., McPhail, K., Cahill, P., *et al.*: 'Efficient subarray realization through layering'. Antenna Applications Symp., Monticello, IL, USA, 2005, pp. 1–35
19 Mailloux, R.J., Santarelli, S., Roberts, T.: 'Polyomino-shaped subarrays for time delay control of planar arrays'. IEEE Antennas and Propagation Society Int. Symp., 2006, pp. 1461–1464
20 Sander, W.: 'Experimental phased-array radar ELRA: antenna system', *IEE Proc. F, Commun. Radar Signal Process.*, 1980, **127**, (4), pp. 285–289
21 Briemle, E.: 'Aspects of adaptive beamforming with an AESA radar with subarray architecture'. IEE Colloquium, Electronic Beam Steering (Ref. No. 1998/481), IET, 1998, pp. 1–4
22 Makino, S., Kadoguchi, S., Betsudan, S.-i., *et al.*: 'An aperiodic array antenna using diamond tiles as subarrays'. EuCAP, Third European Conf., Antennas and Propagation, IEEE, 2009, pp. 3479–3482

doi: 10.1049/iet-map.2014.0308

23 Pierro, V., Galdi, V., Castaldi, G., *et al.*: 'Radiation properties of planar antenna arrays based on certain categories of aperiodic tilings', *IEEE Trans. Antennas Propag.*, 2005, **53**, (2), pp. 635–644
24 Spence, T.G., Werner, D.H.: 'Design of broadband planar arrays based on the optimization of aperiodic tilings', *IEEE Trans. Antennas Propag.*, 2008, **56**, (1), pp. 76–86
25 Morabito, A.F., Isernia, T., Labate, M.G., *et al.*: 'Direct radiating arrays for satellite communications via aperiodic tilings', *Prog. Electromagn. Res.*, 2009, **93**, pp. 107–124
26 Roberts, T.M., Santarelli, S.G., Mailloux, R.J.: 'Method and apparatus for wideband planar arrays implemented with a polyomino subarray architecture'. US Patent 8077109, December 2011
27 Goffer, A.P., Kam, M., Herczfeld, P.R.: 'Design of phased arrays in terms of random subarrays', *IEEE Trans. Antennas Propag.*, 1994, **42**, (6), pp. 820–826
28 Roberts, T.M., Santarelli, S.G., Mailloux, R.J.: 'Efficient ranking of polyomino-based antennas'. IEEE Antennas and Propagation Society Int. Symp., 2007, pp. 5873–5876
29 Brookner, E.: 'Phased arrays and radars past, present and future', *Microw. J.*, 2006, **49**, (1), p. 24
30 Mailloux, R.J., Santarelli, S., Roberts, T., *et al.*: 'Irregular polyomino-shaped subarrays for space-based active arrays', *Int. J. Antennas Propag.*, 2009, **2009**, pp. 1–9
31 Scholnik, D.P., Coleman, J.O.: 'Optimal array-pattern synthesis for wideband digital transmit arrays', *IEEE J. Sel. Top. Signal Process.*, 2007, **1**, (4), pp. 660–677
32 Zatman, M.: 'Digitization requirements for digital radar arrays'. IEEE Int. Radar Conf., 2001, pp. 163–168
33 Nickel, U.R.: 'Spotlight music: super-resolution with subarrays with low calibration effort', *IEE Proc., Radar Sonar Navig.*, 2002, **149**, (4), pp. 166–173
34 Haupt, R.L., Aten, D.: 'Low sidelobe arrays via dipole rotation', *IEEE Trans. Antennas Propag.*, 2009, **57**, (5), pp. 1575–1579
35 Woelder, K., Granholm, J.: 'Cross-polarization and sidelobe suppression in dual linear polarization antenna arrays', *IEEE Trans. Antennas Propag.*, 1997, **45**, (12), pp. 1727–1740
36 Granholm, J., Woelders, K.: 'Dual polarization stacked microstrip patch antenna array with very low cross-polarization', *IEEE Trans. Antennas Propag.*, 2001, **49**, (10), pp. 1393–1402

8 Appendix

A theorem is given here to obtain the optimal phase shift values at subarray level.

Theorem: A function $f: \mathbb{R}^n \to \mathbb{C}$ is defined as

$$f(\boldsymbol{x}) = \sum_{i=1}^{n} [\rho_i \, \mathrm{e}^{\mathrm{j}(\overline{\theta}+x_i)}] \tag{24}$$

where $\rho_i \geq 0$ for $\forall i \in \{1, \ldots, n\}$ and $\sum_{i=1}^{n} \rho_i \neq 0$, $\overline{\theta} = \left(\sum_{i=1}^{n} (\rho_i \theta_i) / \sum_{i=1}^{n} \rho_i\right)$, $\theta_i = \overline{\theta} + x_i$. Then the first-order approximation of f at the point $\mathbf{0}$ is

$$\sum_{i=1}^{n} \rho_i \, \mathrm{e}^{\mathrm{j}\overline{\theta}} \tag{25}$$

Proof: According to the definition of f, we have

$$\begin{aligned} f(\boldsymbol{x}) &= \mathrm{e}^{\mathrm{j}\overline{\theta}} \sum_{i=1}^{n} (\rho_i \, \mathrm{e}^{\mathrm{j}x_i}) \\ &= \mathrm{e}^{\mathrm{j}\overline{\theta}} \sum_{i=1}^{n} \rho_i (1 + \mathrm{j}x_i + O(x_i^2)) \\ &= \sum_{i=1}^{n} \rho_i \, \mathrm{e}^{\mathrm{j}\overline{\theta}} + \mathrm{j} \sum_{i=1}^{n} \rho_i x_i \, \mathrm{e}^{\mathrm{j}\overline{\theta}} + \sum_{i=1}^{n} O(x_i^2) \end{aligned} \tag{26}$$

where $O(x_i^2)$ is the infinitesimal of the same order of x_i^2. Note that

$$\sum_{i=1}^{n} \rho_i x_i = \sum_{i=1}^{n} \rho_i (\theta_i - \overline{\theta}) = \sum_{i=1}^{n} \rho_i \overline{\theta} - \sum_{i=1}^{n} \rho_i \overline{\theta} = 0 \tag{27}$$

and

$$\sum_{i=1}^{n} O(x_i^2) = O(\|\boldsymbol{x}\|^2) \tag{28}$$

Therefore

$$f(\boldsymbol{x}) = \sum_{i=1}^{n} \rho_i \, \mathrm{e}^{\mathrm{j}\overline{\theta}} + O(\|\boldsymbol{x}\|^2) \tag{29}$$

Therefore $\sum_{i=1}^{n} \rho_i \, \mathrm{e}^{\mathrm{j}\overline{\theta}}$ is the first-order approximation of $f(\boldsymbol{x})$ at $\mathbf{0}$. □